

# Photodissociation of Alkyl Nitrites in a Molecular Beam. Primary and Secondary Reactions

C. S. Effenhauser, P. Felder, and J. Robert Huber\*

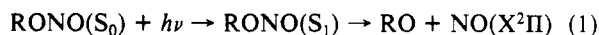
Physikalisch-Chemisches Institut der Universität Zürich Winterthurerstrasse 190, CH-8057 Zürich, Switzerland (Received: April 21, 1989; In Final Form: July 13, 1989)

The translational energy distributions  $P(E_T)$  for the 248-nm photodissociation products (NO + RO) of isopropyl nitrite and *tert*-butyl nitrite have been measured with a molecular beam time-of-flight (TOF) apparatus. Previous experiments with methyl nitrite and ethyl nitrite have been repeated with higher resolution. The average photofragment translational energies of these four alkyl nitrites are in good agreement with those predicted by an impulsive model that treats the NO as a rigid fragment and the alkoxy radical as a soft fragment. Hence, and in contrast to the vibrational predissociation on the  $S_1$  potential energy surface,  $S_2$  dissociation is direct and involves no significant "vibrational-translational" coupling between the reaction coordinate  $r_{O-N}$  and the  $r_{N=O}$  coordinate. The width of the experimental  $P(E_T)$  distributions decreases with increasing size of the alkoxy substituent. This result is discussed in terms of an anticorrelation between the internal energies of a fragment pair. Furthermore, the spontaneous secondary dissociation of isopropoxy and *tert*-butoxy photofragments was observed which yields  $CH_3$  radicals and acetaldehyde or acetone, respectively. The unimolecular decay of these alkoxy radicals confirms their relatively high internal energy as deduced from the primary  $P(E_T)$  and it is shown that this decay occurs on a submicrosecond time scale.

## Introduction

Photodissociation of isolated molecules can provide the state-specific data that in combination with potential energy surface calculations allows us to gain unprecedented insight into the microscopic decay of a molecule.<sup>1-3</sup> In a series of articles, alkyl nitrites (RONO) have been shown to be very suitable for such mechanistic studies<sup>2</sup> and the bond-breaking processes on the  $S_1$  potential surface of the simplest members of this class of molecules, HONO<sup>4-7</sup> and  $CH_3ONO$ ,<sup>8-10</sup> are now fairly well established.

After excitation into the vibrationally structured first absorption band ( $S_1(n\pi^*) \leftarrow S_0$ ) between 300 and 400 nm, alkyl nitrites dissociate according to the scheme



producing alkoxy and nitric oxide fragments with strongly anisotropic angular distributions. Photofragment translational spectroscopy (TOF),<sup>11-14</sup> resonance-enhanced multiphoton ionization (MPI),<sup>15,16</sup> and laser-induced fluorescence (LIF)<sup>4,5,17-25</sup> have

been used to measure the fragment properties.

The C—O—N=O moiety of alkyl nitrites is planar, allowing us to assign the spectroscopic data using the  $C_s$  symmetry group. The weak  $S_1(n\pi^*, A'') \leftarrow S_0(A')$  transition is out-of-plane and localized on the O—N=O group.<sup>26</sup> The ab initio  $S_1$ -PES possesses a shallow potential well with respect to the pertinent coordinates  $r_{N=O}$  and  $r_{O-N}$  which gives rise to vibrational structure in the absorption spectrum and to a vibrational predissociation mechanism.<sup>9,10</sup> In contrast, the strong  $S_2(A') \leftarrow S_0(A')$  transition is in-plane, is of  $\pi\pi^*$  character, and therefore is delocalized. This assignment was corroborated by measuring a positive anisotropy parameter for the photofragment angular distribution after excitation of the  $S_2$  state at 248 and 193 nm.<sup>13</sup>

The broad structureless absorption with a maximum at  $\sim 220$  nm points to a direct dissociation process. Photodissociation of *tert*-butyl nitrite at 250 nm produced NO fragments predominantly in the vibrational ground state.<sup>27-29</sup> This result is interesting in view of the fact that vibrationally hot alkoxy radicals are known to be produced in the case of ethyl nitrite dissociation since the photofragment TOF spectra indicate that a significant fraction of the ethoxy radicals undergo a unimolecular decay.<sup>14</sup> The observation of vibrationally hot alkoxy radicals and vibrationally cold NO fragments is quite different from the following  $S_1$  dissociation. It thus appears that alkyl nitrites offer a convenient way to study different dissociation mechanisms with the same primary products by simply preparing the parent molecule on either the  $S_1$  or the  $S_2$  PES.

The present work is concerned with the decay mechanism following excitation into the  $S_2$  state at 248 nm. Using a newly designed high-resolution photofragment TOF apparatus, we in-

(1) See articles in *Faraday Discuss. Chem. Soc.* **1986**, 82; **1989**, 8. *Molecular Photodissociation Dynamics*, Bagott, J., Ashfold, M. N. R., Eds.; Royal Society of Chemistry: London, 1987.

(2) Reisler, H.; Noble, M.; Wittig, C. In *Molecular Photodissociation Dynamics*; Bagott, J., Ashfold, M. N. R., Eds.; Royal Society of Chemistry: London, 1987.

(3) Hall, G. E.; Houston, P. L., to be submitted for publication in *Annu. Rev. Phys. Chem.*

(4) Vasudev, R.; Zare, R. N.; Dixon, R. N. *Chem. Phys. Lett.* **1983**, 96, 399. *J. Chem. Phys.* **1984**, 80, 4863.

(5) Shan, J. H.; Vasudev, R. *Chem. Phys. Lett.* **1987**, 141, 472.

(6) Hennig, S.; Untch, A.; Schinke, R.; Nonella, M.; Huber, J. R. *Chem. Phys.* **1989**, 129, 93.

(7) Suter, H. U.; Huber, J. R. *Chem. Phys. Lett.* **1989**, 155, 203.

(8) Huber, J. R. *Pure Appl. Chem.* **1988**, 60, 947.

(9) Nonella, M.; Huber, J. R. *Chem. Phys. Lett.* **1986**, 131, 376. Hennig, S.; Engel, V.; Schinke, R.; Nonella, M.; Huber, J. R. *J. Chem. Phys.* **1987**, 87, 3522.

(10) Nonella, M.; Huber, J. R.; Untch, A.; Schinke, R. *J. Chem. Phys.* **1989**, 91, 194.

(11) Tuck, A. F. *J. Chem. Soc., Faraday Trans. 2* **1977**, 73, 689.

(12) Keller, B. A.; Felder, P.; Huber, J. R. *J. Phys. Chem.* **1987**, 91, 114.

(13) Felder, P.; Keller, B. A.; Huber, J. R. *Z. Phys. D* **1987**, 6, 185.

(14) Felder, P.; Keller, B. A.; Effenhauser, C. S. *Ber. Bunsen-Ges. Phys. Chem.* **1988**, 92, 426.

(15) Inoue, G.; Kawasaki, M.; Sato, H.; Kikuchi, T.; Kobayashi, S.; Arakawa, T. *J. Chem. Phys.* **1987**, 87, 5722.

(16) Winniczek, J. W.; Dubs, R. L.; Appling, J. R.; Mc Koy, V.; White, M. G. *J. Chem. Phys.* **1989**, 90, 949.

(17) Lahmani, F.; Lardeux, C.; Solgadi, D. *Chem. Phys. Lett.* **1983**, 102, 523.

(18) Benoist d'Azy, D.; Lahmani, F.; Lardeux, C.; Solgadi, D. *Chem. Phys.* **1985**, 94, 247.

(19) Lahmani, F.; Lardeux, C.; Solgadi, D. *Chem. Phys. Lett.* **1986**, 129, 26.

(20) Brühlmann, U.; Dubs, M.; Huber, J. R. *J. Chem. Phys.* **1987**, 86, 1294.

(21) Brühlmann, U.; Huber, J. R. *Z. Phys. D* **1987**, 7, 1.

(22) Docker, M. P.; Ticktin, A.; Brühlmann, U.; Huber, J. R. *J. Chem. Soc., Faraday Trans. 2*, in press.

(23) Ticktin, A.; Huber, J. R. *Chem. Phys. Lett.*, in press.

(24) Schwartz-Lavi, D.; Bar, I.; Rosenwaks, S. *Chem. Phys. Lett.* **1986**, 128, 123.

(25) Lavi, R.; Schwartz-Lavi, D.; Bar, I.; Rosenwaks, S. *J. Phys. Chem.* **1987**, 91, 5398.

(26) Calvert, J. G.; Pitts, J. N., Jr. *Photochemistry*; Wiley: New York, 1966.

(27) Schwartz-Lavi, D.; Rosenwaks, S. *J. Chem. Phys.* **1988**, 88, 6922.

(28) August, J.; Brouard, M.; Docker, M. P.; Milne, C. J.; Simons, J. P.; Lavi, R.; Rosenwaks, S.; Schwartz-Lavi, D. *J. Phys. Chem.* **1988**, 92, 5485.

(29) Brühlmann, U.; Ticktin, A.; Docker, M. P.; Huber, J. R., to be submitted for publication.

vestigated the translational energy distributions of the primary photofragments formed upon dissociation of isopropyl nitrite (IPN) and *tert*-butyl nitrite (TBN) and repeated our previous, lower resolution, measurements on ethyl nitrite (ETN)<sup>14</sup> and methyl nitrite (MEN).<sup>12</sup> Furthermore, the unimolecular decay of the hot alkoxy radicals that emerge from the IPN and TBN dissociation was also explored by the TOF technique. These measurements furnished additional information on the energy partitioning in the primary decay and provided data to elucidate the dominant secondary decay processes.

### Experimental Section

The experiments were carried out on a molecular beam apparatus with a rotating pulsed molecular beam source.<sup>30</sup> Photodissociation was induced by unpolarized light pulses from a KrF excimer laser (Lambda Physik EMG 101 MSC) directed along the rotation axis of the molecular beam source. The neutral photofragments produced at the intersection of the two beams were ionized after a flight path of 34.5 cm and detected with a quadrupole mass spectrometer (Balzers QMA 160) equipped with a paraxial secondary electron multiplier. The ions were counted with a multichannel scaler which utilizes 800 channels with 1- $\mu$ s dwell time. The pulsed molecular beam valve, the laser pulse, and the scaler were synchronized by a microprocessor (INTEL 2732) linked to an ATARI ST 1040 microcomputer. The detector system was housed in a triply differentially pumped UHV chamber at a pressure of approximately  $10^{-10}$  mbar. The pulsed molecular beam was generated by a piezoelectric valve (0.3-mm orifice) operated at a repetition rate of 30 Hz. In all experiments a 5% mixture of alkyl nitrite seeded in He or Ne was expanded at a stagnation pressure of 400 mbar. Under these conditions clusters did not contribute to the TOF signal. The velocity distribution in the molecular beam was periodically measured by the laser-induced hole burning method, yielding a most probable beam velocity of 1200 and 780  $\text{ms}^{-1}$  for He and Ne carrier gas, respectively. *tert*-Butyl nitrite was obtained from Fluka AG, Buchs, and used without further purification. IPN, ETN, and MEN were synthesized according to a published procedure<sup>31</sup> and purified by vacuum distillation.

To evaluate the translational energy distributions in the primary reaction, the TOF distributions of the NO fragments were measured at the mass filter setting  $m/e = 30$  by averaging over 50 000 laser shots. In addition, TOF distributions at  $m/e = 15, 29, 43,$  and  $58$ , related to the alkoxy radicals and their secondary dissociation products, were measured when investigating the photodissociation of IPN and TBN. The low signal to noise (S/N) ratio required an accumulation of up to 200 000 laser shots. All experimental TOF distributions were subject to a small time offset due to the transit time of the ions through the mass filter. This ion flight time is proportional to the square root of the  $m/e$  ratio. The proportionality constant for singly charged ions was determined to be  $3.7 \mu\text{s} (\text{amu})^{-1/2}$ .

### Results

Figures 1 and 3 display the TOF distributions of NO photofragments ( $m/e = 30$ ) from IPN and TBN seeded in helium and measured at detection angles  $\theta_L = 24^\circ$  and  $60^\circ$ . Furthermore, TOF spectra from beams with neon as carrier gas were recorded at  $\theta_L = 24^\circ$  and  $72^\circ$  and are shown in Figures 2 and 4. The center-of-mass (CM) translational energy distribution  $P(E_T)$  was obtained by fitting calculated TOF distributions, which were computed with a trial  $P(E_T)$  function, to the measured ones. This calculation takes into account the transformation from the laboratory to the CM reference frame and various broadening effects, namely the size of the laser spot ( $2 \times 2 \text{ mm}^2$ ), the angular divergence of the molecular and photofragment beams ( $2.2^\circ$  and  $0.8^\circ$ , respectively), the effective ionizer length (4 mm), and the velocity distribution of the molecular beam. The calculated TOF

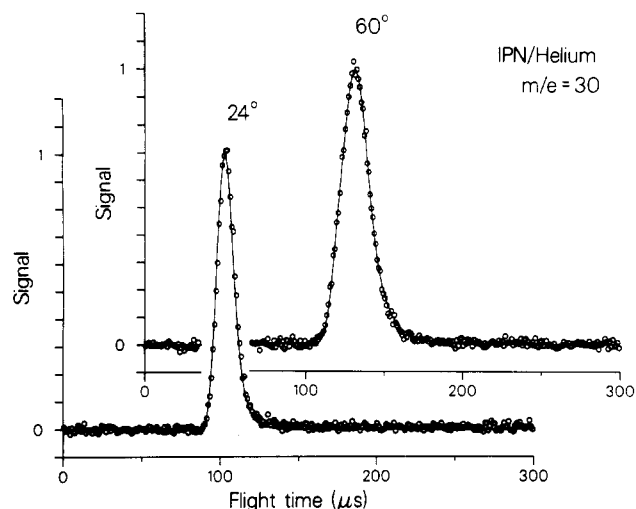


Figure 1. TOF distributions of IPN at  $m/e = 30$  measured at the detection angles  $\theta_L = 24^\circ$  and  $60^\circ$  with helium as carrier gas. The solid lines are calculated from the  $P(E_T)$  function shown in Figure 5. The time axis is corrected for the ion flight time.

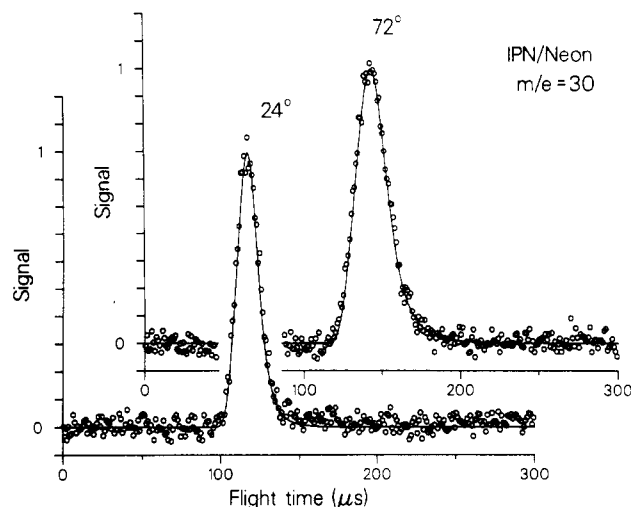


Figure 2. TOF distributions of IPN at  $m/e = 30$  measured at the detection angles  $\theta_L = 24^\circ$  and  $72^\circ$  with neon as carrier gas. The solid lines are calculated from the  $P(E_T)$  function shown in Figure 5.

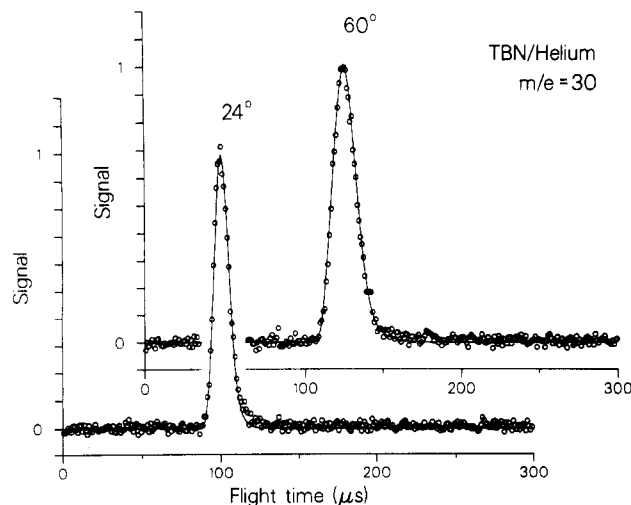
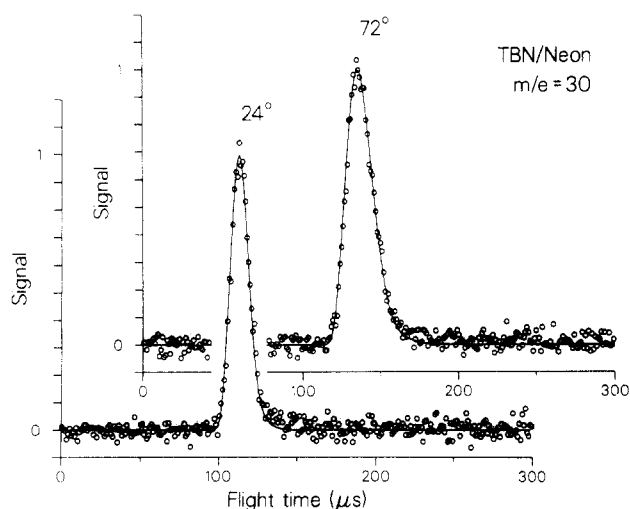


Figure 3. TOF distribution of TBN at  $m/e = 30$  measured at the detection angles  $\theta_L = 24^\circ$  and  $60^\circ$  with helium as carrier gas. The solid lines are calculated from the  $P(E_T)$  distribution shown in Figure 5.

distributions are shown in Figures 1–4 (solid lines). The associated  $P(E_T)$  functions are displayed in Figure 5 along with those obtained for MEN and ETN. For these two molecules TOF frag-

(30) Felder, P., to be submitted for publication.

(31) *Organic Syntheses*; Blatt, A. H., Ed.; Wiley: New York, 1943; Collect. Vol. 2, p 204.



**Figure 4.** TOF distributions of TBN at  $m/e = 30$  measured at the detection angles  $\theta_L = 24^\circ$  and  $72^\circ$  with neon as carrier gas. The solid lines are calculated from the  $P(E_T)$  function shown in Figure 5.

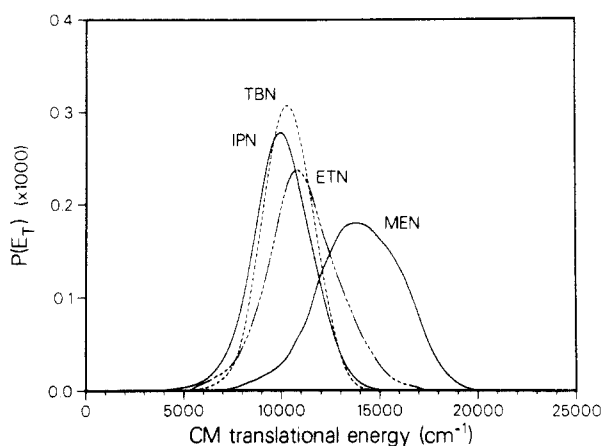


**Figure 5.** CM translational energy distributions for alkyl nitrite photodissociation at 248 nm. The  $P(E_T)$  distribution functions are normalized to unity and refer to both fragments.

ment distributions for  $m/e = 30$  were recorded at the detection angles  $\theta_L = 24^\circ, 60^\circ,$  and  $95^\circ$ .

The fact that each  $P(E_T)$  was determined by simultaneously fitting several TOF distributions measured under different kinematic conditions increases the reliability of the  $P(E_T)$  functions considerably. The pertinent parameters of the  $P(E_T)$  are listed in Table I. The remeasured  $P(E_T)$  distributions of MEN and ETN are shifted to higher energies by about 500 and 1000  $\text{cm}^{-1}$ , respectively, as compared to the earlier low-resolution experiments.<sup>12,14</sup> We believe that the differences are due to a less accurate determination of the beam velocity in the previous study using fast ionization gauges. The  $P(E_T)$  distributions (cf. Figure 5) are approximately symmetrical and of similar shape which justifies the use of full width at half maximum (fwhm) values listed in Table I for their specification and comparison.

To give an impression of the error limits of our experimental fwhm values, Figure 6 shows an example for TOF distributions calculated from a broader (fwhm = 3600  $\text{cm}^{-1}$ ) and a narrower (fwhm = 2600  $\text{cm}^{-1}$ )  $P(E_T)$  than the one obtained from the best fit (fwhm = 3100  $\text{cm}^{-1}$ ). It is evident that these TOF distributions do not represent the experimental data well. The deviation allows us to estimate an error limit for our fwhm values of  $\pm 200 \text{ cm}^{-1}$ .

The TOF distributions of alkoxy radicals formed upon photodissociation of IPN and TBN were measured at several  $m/e$  settings. Typical examples are shown in Figures 8 and 9 for a detection angle of  $24^\circ$ . At  $m/e = 15$  methyl ions (and a small amount of doubly charged NO ions) are detected. The spectra contain fast signals that cannot be assigned to methyl ions formed from the corresponding alkoxy radicals by fragmentation in the

**TABLE I: Translational Energy Distributions in the 248-nm Photodissociation of Alkyl Nitrites and Predictions of the Combined Impulsive Model<sup>a</sup>**

	MEN	ETN	IPN	TBN
Experiment				
$E_T^b$	14000 (0.55)	11100 (0.43)	9900 (0.39)	10200 (0.40)
fwhm <sup>c</sup>	5300	3700	3300	3100
$E_I^d$	11700 (0.45)	14600 (0.57)	15800 (0.61)	15500 (0.60)
Combined Impulsive Model				
$E_T^e$	13100 (0.51)	11100 (0.43)	10000 (0.39)	9400 (0.37)

<sup>a</sup>All energies refer to both fragments and the energy unit is  $\text{cm}^{-1}$ . A constant  $E_{\text{avl}} = 25700 \text{ cm}^{-1}$  was used for all alkyl nitrites. The numbers in parentheses are fractions of  $E_{\text{avl}}$ . <sup>b</sup>Average CM translational energy. <sup>c</sup>Full width at half maximum values of the corresponding  $P(E_T)$  distributions. <sup>d</sup>Average internal energy of both fragments calculated from energy conservation. <sup>e</sup>The structural data for the free parent molecules were taken from ref 34.

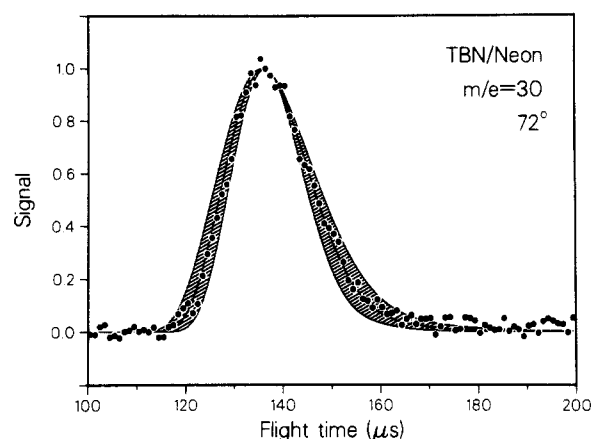


**Figure 6.** TOF distribution (points) of TBN at  $m/e = 30, \theta_L = 72^\circ$ . The border lines of the shaded area are calculated from  $P(E_T)$  distributions whose fwhm values are 500  $\text{cm}^{-1}$  wider and narrower than that of the original  $P(E_T)$  shown in Figure 5.

ionizer. By use of the conservation of linear momentum, the flight times for the alkoxy radicals predicted from the  $m/e = 30$  spectra were found to be much longer, as indicated by the arrows in Figures 8 and 9. The fast TOF components are attributed to an extensive unimolecular decay of the alkoxy radicals which are formed in the primary reaction. As will be discussed in the following section, the TOF distributions at  $m/e = 43$  support this claim of a secondary decay. A small contribution from surviving alkoxy radicals is evident at  $m/e = 43$  as identified via linear momentum conservation, but no signal was detected at the parent masses of isopropoxy and *tert*-butoxy ( $m/e = 59$  and  $73$ , respectively). This fact is attributed to a fragmentation of the surviving alkoxy radicals in the ionizer.

## Discussion

**1. Primary Dissociation.** The results of the translational energy measurements of the photofragments are summarized in Table I. The average of the total translational energy  $E_T$  of both fragments is larger in MEN (14000  $\text{cm}^{-1}$ ) than in ETN (11000  $\text{cm}^{-1}$ ) and is approximately the same for IPN (9900  $\text{cm}^{-1}$ ) and TBN (10200  $\text{cm}^{-1}$ ). Since the internal energy of the parent molecules is negligible in the cold supersonic beam ( $T_{\text{rot}} \sim 10 \text{ K}$ ) and the dissociation energy  $D_0 = 14600 \pm 400 \text{ cm}^{-1}$  is about the same for the four alkyl nitrites within experimental error,<sup>32,33</sup> the available energy  $E_{\text{avl}} = h\nu - D_0$  of  $\sim 25700 \pm 500 \text{ cm}^{-1}$  can be taken as identical for these nitrites. Accordingly, the measured  $E_T$  values correspond to 55% (MEN), 41% (ETN), 39% (IPN), and 40% (TBN) of  $E_{\text{avl}}$ , respectively. The internal energy of both fragments, which comprises the rotational and vibrational energy

(32) Batt, L. *Int. J. Chem. Kinet.* **1979**, *11*, 977, and references cited therein.

(33) For a review, see Heicklen, J. P. *Adv. Photochem.* **1988**, *14*, 177.

$E_1 = E_{\text{avl}} - E_T$ , increases from 11 700  $\text{cm}^{-1}$  ( $\sim 45\%$ ) in MEN to about 15 000  $\text{cm}^{-1}$  ( $\sim 60\%$ ) in ETN, IPN, and TBN. The internal energy distribution is reflected by the shape of  $P(E_T)$ . It is surprising that the width of  $P(E_T)$  decreases with increasing size of the alkyl substituent i.e. the fwhm value decreases from 5300  $\text{cm}^{-1}$  in MEN to about 3100  $\text{cm}^{-1}$  in TBN.

An interpretation of the results on the basis of accurate potential energy surfaces is not yet possible for the alkyl nitrites studied in this work. Even for a small molecule like MEN in its first electronically excited state, an ab initio calculation of the PES still requires a formidable computational effort although in this case the dimensionality can be reduced to a small number of relevant coordinates such as  $r_{\text{N=O}}$ ,  $r_{\text{O-N}}$ , and the ONO angle.<sup>7,10</sup> For the  $S_2$  photodissociation the situation is, however, more complicated due to the delocalized nature of the  $S_2 \leftarrow S_0$  transition which requires consideration of a greater number of coordinates.

Under these circumstances, and given the fact that the dissociation process is fast as indicated by the broad structureless  $S_2 \leftarrow S_0$  absorption (B), we first applied the impulsive model to gain information about the  $S_2$ -PES. This crude model treats photo-fragmentation as a quasi-diatomic bond-breaking process induced by a steep repulsive potential that is suddenly switched on between the atoms of the dissociating bond. Thus, if along the reaction coordinate the potential surface does not act on the excited complex to introduce appreciable bond length and bond angle changes, the impulsive model should reasonably well predict the energy partitioning in the fragments. In its "rigid" or "soft" limit the geometries of the fragments are considered fixed or flexible, respectively.

Having modified the rigid model introduced by Tuck<sup>11</sup> to include the conservation of angular momentum (see Appendix), we chose a combination of the rigid and soft descriptions owing to two experimental facts. First, the efficient secondary dissociation, i.e. the unimolecular decay of the alkoxy radicals following photodissociation, implies that these fragments possess a considerable amount of vibrational energy.<sup>14,32,33</sup> Second, in a recent LIF study on the photodissociation of TBN at 250 nm, it was shown that the NO fragments are produced predominantly in the vibrational ground state (92% in  $v = 0$ ).<sup>27</sup> Therefore, the vibrationally cold NO and the vibrationally hot alkoxy groups are treated as a rigid and a soft moiety, respectively. Table I contains the results in terms of the translational energies  $\langle E_T \rangle$  which agree very well with the experiment.

The correct predictions of the impulsive model in its "soft alkoxy-rigid NO" limit suggest—as does in a direct way the experimental finding of an almost cold NO fragment—that the bond length of the N=O group is not appreciably changed during the dissociation process. The bond length  $r_{\text{N=O}}$  of the parent molecule in the  $S_0$  state is nearly identical with that of the free NO molecule (1.17 Å<sup>34</sup> versus 1.15 Å<sup>35</sup>) which means that  $r_{\text{N=O}}$  in the Franck-Condon region of photoexcitation is close to its asymptotic value after dissociation. The fast and direction dissociation process on the  $S_2$  potential surface does evidently not permit a change in the N=O bond length during dissociation, in contrast to the vibrational predissociation on the  $S_1$  PES. Thus,  $S_2$  dissociation involves no significant translational-vibrational coupling between the reaction coordinate O—N and the N=O coordinate.

To partition the internal energy  $E_1$  given in Table I, the vibrational excitation of NO can be neglected so that  $E_1 = E_{\text{rot}}(\text{NO}) + E_i(\text{RO})$ . The average rotational energy of NO after photo-fragmentation of TBN at 250 nm is  $E_{\text{rot}}(\text{NO}, v = 0) \sim 5100 \text{ cm}^{-1}$ <sup>27</sup> and in the case of MEN it was found to be about 4500  $\text{cm}^{-1}$ .<sup>29</sup> We may, therefore, conclude that for the molecules ETN, IPN, and TBN,  $E_{\text{rot}}(\text{NO}) = E_i(\text{NO}) \sim 5000 \text{ cm}^{-1}$  and that the alkoxy fragments possess the following average internal energies:  $E_i(\text{EtO}) \sim 9600$ ,  $E_i(i\text{-PrO}) \sim 10800$ , and  $E_i(t\text{-BuO}) \sim 10500 \text{ cm}^{-1}$ . In spite of the fact that the number of vibrational degrees

of freedom increases from 18 in EtO to 36 in *t*-BuO, the internal energy contents of the three alkoxy radicals are similar, underlining the nonstatistical character of the dissociation process. With increasing size of the alkoxy moiety a limiting value of  $E_i(\text{RO})$  is evidently approached and an interesting model system emerges that might be used to study spatially oriented "surface-bound" NO molecules.

**2. Correlation Effect.** Next we focus on the translational energy distribution functions. The internal energy  $E_1$  of the photofragments is related to the experimentally determined translational energy  $E_T$  by energy conservation, and the distribution function  $P(E_1)$  is obtained by a reflection of  $P(E_T)$  at  $E = E_{\text{avl}}/2$  where  $E_{\text{avl}}$  is the same for the four nitrites. Hence, the fwhm values listed in table I pertain to both  $P(E_T)$  and  $P(E_1)$ . In the following we denote the internal energy distributions of the two individual fragment species by  $p_1(E_{i,1})$  and  $p_2(E_{i,2})$ .

One notices that the fwhm values decrease with increasing size of the alkyl nitrite. This could mean that either one or both functions  $p_1$  and  $p_2$  become narrower with increasing molecular size. Since it is known from the LIF studies of MEN<sup>29</sup> and TBN<sup>27</sup> that the internal energy distribution of the NO fragment is almost the same (fwhm  $\sim 3000 \text{ cm}^{-1}$ ) in both molecules, and probably also in ETN and IPN, one would have to assume very narrow internal energy distributions for the larger alkoxy radicals to explain our experimental fwhm values. As will be shown later, the  $P$  function measured with the present TOF method is given by a convolution of  $p_1$  and  $p_2$  (eq 4) provided that the internal energies of the fragments are *not* correlated. Since the internal energy distribution of the NO fragment  $p_{\text{NO}}$  is approximately Gaussian shaped<sup>27,29</sup> (and also our  $P$  functions shown in Figure 5), one can easily estimate the fwhm values of the corresponding  $p_{\text{RO}}$  functions to be 4400 (MEN), 2200 (ETN), 1400 (IPN), and 800  $\text{cm}^{-1}$  (TBN) assuming  $p_{\text{NO}}$  and  $p_{\text{RO}}$  are Gaussians. As a consequence, the  $p(E_i)$  of the alkoxy radicals would have to become narrower with increasing size of the alkyl substituent, a quite unrealistic behavior in view of the rapidly increasing number of degrees of freedom. Therefore we consider the possibility that the observed trend is caused by an anticorrelation between  $E_{i,1}$  and  $E_{i,2}$  and use a simple picture to describe the relationship between the distribution functions measured by the TOF and LIF techniques.

In general, the distribution of the fragment internal energies  $E_{i,1}$  and  $E_{i,2}$  can be described in terms of a pair distribution function  $p(E_{i,1}, E_{i,2})$  which contains the correlation between  $E_{i,1}$  and  $E_{i,2}$ . Normalized to unity,  $\int \int p(E_{i,1}, E_{i,2}) dE_{i,1} dE_{i,2} = 1$ , the expression  $p dE_{i,1} dE_{i,2}$  is the probability of finding fragment 1 with the internal energy in the interval  $(E_{i,1}, E_{i,1} + dE_{i,1})$  and simultaneously fragment 2 in the interval  $(E_{i,2}, E_{i,2} + dE_{i,2})$ .

LIF measurements probing rovibrational fragment states can provide the distribution function  $p(E_i)$  of the internal energy of one fragment species. The result of such a LIF experiment corresponds to a projection of  $p(E_{i,1}, E_{i,2})$  onto the  $E_{i,1}$  or  $E_{i,2}$  axis (cf. Figure 7) depending on which fragment is probed, i.e.

$$p_1(E_{i,1}) = \int p(E_{i,1}, E_{i,2}) dE_{i,2}$$

or

$$p_2(E_{i,2}) = \int p(E_{i,1}, E_{i,2}) dE_{i,1} \quad (2)$$

respectively.

In contrast, a TOF experiment yields the translational energy distribution  $P(E_T)$ . As mentioned above,  $P(E_T)$  can be converted to the distribution function of the *sum* of the internal energies of both fragments,  $P(E_1)$ . In terms of the pair distribution function,  $P(E_1)$  is obtained by a projection perpendicular to the diagonal  $E_{i,1} = E_{i,2}$  (cf. Figure 7) i.e.

$$P(E_1) = \int p(E_{i,1}, E_1 - E_{i,1}) dE_{i,1} = \int p(E_1 - E_{i,2}, E_{i,2}) dE_{i,2} \quad (3)$$

In the case of state-selective LIF experiments (Doppler profile measurements of a selected rovibronic fragment state) or TOF

(34) Landolt-Börnstein, New Series II/15, 1987.

(35) Herzberg, G. *Spectra of Diatomic Molecules*, 2nd ed.; Van Nostrand Reinhold Company: New York, 1950.

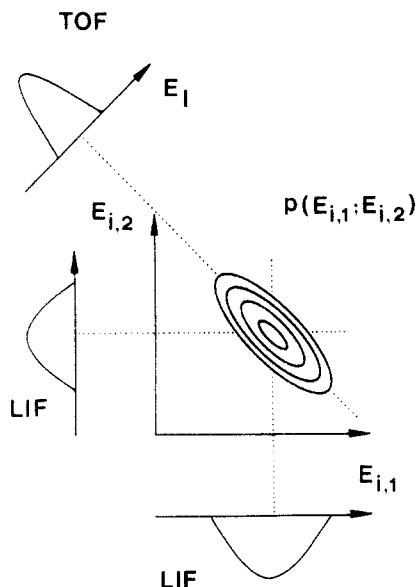


**Figure 7.** Example of a pair distribution function featuring anticorrelation between the internal energies of the fragments. The pair distribution function  $p(E_{i,1}; E_{i,2})$  is shown as a contour plot. The internal energies of the fragments are denoted with  $E_{i,1}$  and  $E_{i,2}$  and the total internal energy with  $E_1$ . The different projections of  $p$  yielding the  $p_1$ ,  $p_2$ , and  $P$  distribution functions as measured with LIF and TOF experiments, respectively, are shown. (Note that the scale of  $E_1$  is compressed by a factor of  $\sqrt{2}$  as compared to that of  $E_{i,1}$  and  $E_{i,2}$ .)

experiments (using state-selective MPI of a fragment<sup>36</sup>) the result is given by a section through the pair distribution function.

Figure 7 shows a simple example where we used an arbitrary function,  $p(E_{i,1}, E_{i,2})$ , which features anticorrelation between  $E_{i,1}$  and  $E_{i,2}$ . The example illustrates the effect of an internal energy anticorrelation on  $P(E_1)$ ,  $p_1(E_{i,1})$ , and  $p_2(E_{i,2})$  as measured either by the LIF or TOF techniques. If strong anticorrelation prevails,  $P(E_1)$  can become narrower than each of the individual  $p_1(E_{i,1})$  and  $p_2(E_{i,2})$  distributions, while for uncorrelated  $E_{i,1}$  and  $E_{i,2}$  the function  $P(E_1)$  is broader than both  $p_1(E_{i,1})$  and  $p_2(E_{i,2})$  since it is given by the convolution

$$P(E_1) = \int p_1(E_{i,1})p_2(E_1 - E_{i,1}) dE_{i,1} \quad (4)$$

This relationship could be a convenient way to extract the  $p_1(E_{i,1})$  distribution of one fragment if  $p_2(E_{i,2})$  and  $P(E_1)$  are known from simple LIF or TOF experiments and the internal energies are not correlated.

On the basis of these considerations in connection with the above-mentioned experimental findings<sup>27-29</sup> the surprising trend found in the fwhm values of Table I indicates that internally cold NO fragments are preferentially produced in coincidence with hot alkoxy radicals and vice versa. Furthermore, it illustrates that caution should be applied when comparing the widths of fragment energy distributions obtained by different experimental methods even when the distribution functions have the same shape.

**3. Secondary Dissociation.** In the previous section we have shown that after photofragmentation of ETN, IPN, and TBN at 248 nm the alkoxy radicals possess an average internal energy of about  $10\,000\text{ cm}^{-1}$  ( $\sim 120\text{ kJ mol}^{-1}$ ). This energy content is expected to initiate a further decay of the fragment as has been discussed in works on the gas phase photolysis of alkyl nitrites<sup>32,33</sup> and in a preliminary analysis of TOF fragment distributions of ETN.<sup>14</sup> Here we discuss the secondary dissociation of IPN and TBN which is anticipated to yield methyl radicals and acetaldehyde or acetone according to the schemes

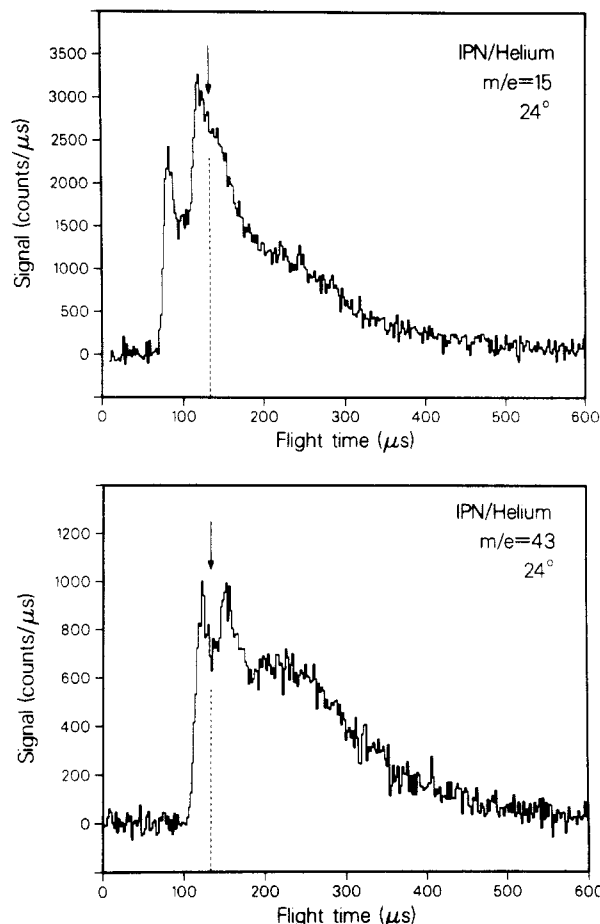
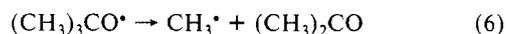


**Figure 8.** TOF distributions of IPN at  $m/e = 15$  (top) and  $m/e = 43$  (bottom) at  $\theta_L = 24^\circ$ . The arrow and the dotted line indicate the shortest possible flight time for surviving alkoxy radicals calculated from linear momentum conservation (see text).

Both reactions are only slightly endothermic with  $\Delta H^\circ_{298} = 23.4\text{ kJ mol}^{-1}$  ( $2000\text{ cm}^{-1}$ ) for reaction 5 and  $\Delta H^\circ_{298} = 29.3\text{ kJ mol}^{-1}$  ( $2500\text{ cm}^{-1}$ ) for reaction 6. In both cases an activation energy of about  $71\text{ kJ mol}^{-1}$  ( $6000\text{ cm}^{-1}$ ) has been deduced from gas kinetic data<sup>32,33</sup> which is considerably smaller than the  $\sim 120\text{ kJ mol}^{-1}$  ( $10\,000\text{ cm}^{-1}$ ) average internal energy of the alkoxy radicals. Moreover, the combined impulsive model, reproducing very well the internal energy of  $(\text{CH}_3)_3\text{CO}^*$  to be  $9750\text{ cm}^{-1}$ , predicts a partitioning of  $E_{\text{vib}} = 6250\text{ cm}^{-1}$  and  $E_{\text{rot}} = 3500\text{ cm}^{-1}$ . Since the rotational energy should contribute at least partially to promote the unimolecular decay, it is expected that most of the alkoxy radicals undergo the secondary decomposition of eq 5 or 6. Under these conditions several thousand wavenumbers are available for the recoil of the secondary fragments.

The features of the TOF distributions taken at  $m/e = 15$  and 43 and displayed in Figure 8 for IPN and Figure 9 for TBN provide strong evidence for reactions 5 and 6 to occur under collision-free conditions. Alkoxy radicals produced in the primary reaction contribute to the TOF spectra by their daughter ions formed in the electron bombardment ionizer. The arrows given in Figures 8 and 9 mark the high-energy threshold of the primary  $P(E_T)$  distribution (Figure 5) and indicate the earliest arrival time for which surviving alkoxy radicals can be expected. The sharp peaks at shorter flight times are attributed to products of the secondary dissociation which recoil in the forward direction (with respect to the velocity vector of the alkoxy radical), whereas the broad shoulder at long flight times corresponds to backward recoiling products.

A more detailed consideration of the features of the TOF distribution spectra leads to the following results. Monitoring  $m/e = 15$ , the sharp peak appearing at  $80\text{ }\mu\text{s}$  in Figures 8 and 9 can be assigned to methyl radicals formed in reactions 4 and 5. The strong peak that appears at a later time,  $\sim 120\text{ }\mu\text{s}$  in the case of

(36) Ogorzalek-Loo, R.; Hall, G. E.; Haerri, H.-P.; Houston, P. L. *J. Phys. Chem.* **1988**, *92*, 5.

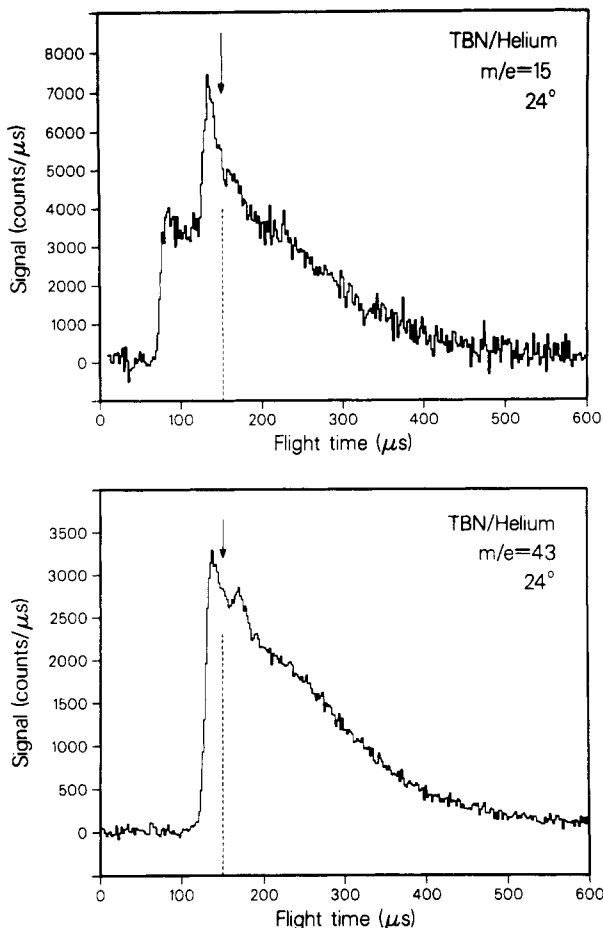


**Figure 9.** TOF distributions of TBN at  $m/e = 15$  (top) and  $m/e = 43$  (bottom) at  $\theta_L = 24^\circ$ . The shortest possible flight time for surviving alkoxy radicals is indicated.

IPN and  $\sim 135 \mu\text{s}$  in that of TBN, is attributed to  $\text{CH}_3^+$  ions formed from the heavier secondary fragments acetaldehyde and acetone in the detector. These products also yield  $\text{CH}_3\text{CO}^+$  ions which give rise to prominent peaks in the TOF spectra monitored at  $m/e = 43$  as also shown in Figures 8 and 9. In the latter, the maxima near  $150 \mu\text{s}$  (IPN) and  $170 \mu\text{s}$  (TBN) match with the linear momentum of the NO fragment and must therefore originate from surviving alkoxy radicals. The simultaneous detection of dissociating and "stable" alkoxy radicals gives some indication of the lifetimes of these species.

In our experiment a primary photofragment is detected as "stable" if it survives on its way to the ionizer which in the present case takes about  $100 \mu\text{s}$  or more. In contrast, the detection of secondary products requires that these be formed within the geometrical acceptance cone of the detector which in our apparatus implies that the secondary dissociation should occur on a time scale of microseconds or less. Alkoxy radicals with a unimolecular decay time in the range  $10\text{--}100 \mu\text{s}$  will, however, not contribute significantly to either the primary or secondary TOF signal. In view of this fact we have estimated the lifetime for the *tert*-butoxy radical as a function of internal energy by means of a series of microcanonical RRKM calculations.<sup>37</sup> The molecular parameters describing the transition state were chosen to yield the experimentally determined preexponential factor of  $\log A = 15.5$ .<sup>32</sup> These calculations show that even when *tert*-butoxy radicals possess an internal energy of merely a few hundred wavenumbers above the activation barrier, the decay takes place on a time scale that is much faster than  $1 \mu\text{s}$ . (The smaller isopropoxy and ethoxy radicals are calculated to decay even faster.) Consequently, a major fraction of the alkoxy radicals produced in the primary reaction is detected in the form of their decay products, whereas the other fraction is detected as "stable" alkoxy radicals. The

observation of stable *tert*-butoxy and isopropoxy radicals implies that the respective internal energy distributions  $p(E_i)$  extend to energies below the activation barrier of the secondary decay. Moreover, a broad  $p(E_i)$  for the alkoxy radicals from IPN and TBN photodissociation is consistent with the anticorrelation effect proposed in the preceding section.

### Summary

1. The photofragment translational energy distributions for the primary dissociation reactions of MEN, ETN, IPN, and TBN at  $248 \text{ nm}$  have been determined. The average translational energies  $\langle E_T \rangle$  amount to  $14000 \text{ cm}^{-1}$  (MEN),  $11000 \text{ cm}^{-1}$  (ETN), and  $\sim 10000 \text{ cm}^{-1}$  in IPN and TBN.

2. The experimental  $\langle E_T \rangle$  values are best reproduced by an impulsive model that assumes a soft alkoxy and a rigid NO moiety. This model is consistent with the small vibrational excitation found by LIF spectroscopy of the NO photofragments.<sup>27</sup> It is thus concluded that  $S_2$  photodissociation occurs on a repulsive potential energy surface with a negligible coupling between the dissociation coordinate and the NO bond length coordinate. This finding is in contrast to the predissociative mechanism on the  $S_1$  surface.<sup>8-10</sup>

3. The average internal energies of the alkoxy radicals are estimated as  $7000 \text{ cm}^{-1}$  (MEN) and  $\sim 10000 \text{ cm}^{-1}$  for the three larger nitrites. These values were obtained from the measured  $\langle E_T \rangle$  by setting up the appropriate energy balances and incorporating spectroscopic results for the internal energy of the NO fragments.

4. Our photofragment TOF distributions show clear evidence for the collisionless unimolecular decay of isopropoxy and *tert*-butoxy radicals formed in the primary dissociation of IPN and TBN. The average internal energy of the RO radicals is well above the activation barrier for the secondary dissociation. Consequently, the latter occurs for most of the alkoxy radicals and proceeds on a submicrosecond time scale.

5. The widths of the translational energy distributions are found to decrease with increasing size of the alkyl nitrite. This surprising fact is attributed to an anticorrelation between the internal energies of a fragment pair, which means that cold NO molecules are preferentially produced in coincidence with hot alkoxy radicals and vice versa.

### Appendix

*Corrected Version of the Rigid Impulsive Model.* In his TOF study of the photolysis of ETN, Tuck<sup>11</sup> extended the impulsive model<sup>38</sup> to the case of two di- or polyatomic fragments. In its rigid limit, Tuck's model does not satisfy the conservation of angular momentum and therefore we have derived a corrected version.

If one denotes the separating fragments with A and B, and the atoms between which the bond breaks with C and D (where atom C belongs to fragment A and atom D to fragment B), the rotational energy of fragment A is

$$E_{\text{rot,A}} = E_{\text{avl}} \left\{ 1 + \frac{I_A((1/\mu_{A,B}) + (r_{\text{CM,B}}^2 \sin^2 \chi_B / I_B))}{r_{\text{CM,A}}^2 \sin^2 \chi_A} \right\}^{-1}$$

and the total translational energy

$$E_T = E_{\text{avl}} - E_{\text{rot,A}} - E_{\text{rot,B}}$$

$$E_T = E_{\text{avl}} \left\{ 1 + \mu_{A,B} \left( \frac{r_{\text{CM,A}}^2 \sin^2 \chi_A}{I_A} + \frac{r_{\text{CM,B}}^2 \sin^2 \chi_B}{I_B} \right) \right\}^{-1}$$

Here,  $\mu_{A,B}$  is the reduced mass of the fragments A and B,  $E_{\text{avl}}$  is the available energy, and  $r_{\text{CM,A}}$  and  $r_{\text{CM,B}}$  denote the absolute values of the vectors  $\vec{r}_{\text{CM,A}}$  and  $\vec{r}_{\text{CM,B}}$  connecting the centers-of-mass of the fragments A and B with the atoms C and D, respectively.  $I_A$  and  $I_B$  are the moments of inertia of the fragments A and B

(37) Bunker, D. L.; Hase, W. L. *QCPE* 234, University of Indiana.

(38) Holdy, K. E.; Klotz, L. C.; Wilson, K. R. *J. Chem. Phys.* **1970**, *52*, 4588.

for rotation around the axis defined by the corresponding angular momenta  $\vec{J}_A = \vec{r}_{CM,A} \times \vec{p}$  and  $\vec{J}_B = \vec{r}_{CM,B} \times \vec{p}$ , respectively ( $\vec{p}$  is the linear momentum of the fragments).  $\chi_A$  and  $\chi_B$  refer to the angle between the vectors  $\vec{r}_{CM,A}$  and  $\vec{r}_{CM,B}$ , respectively, and  $\vec{p}$ .

*Acknowledgment.* This work was supported by the Schweizer Nationalfonds zur Förderung der wissenschaftlichen

Forschung. We thank Dr. M. P. Docker for critically reading the manuscript and Mr. R. Pfister for synthesizing the alkyl nitrites.

**Registry No.** IPN, 541-42-4; TBN, 540-80-7; ETN, 109-95-5; MEN, 624-91-9; EtO, 2154-50-9; *i*-PrO, 3958-66-5; *t*-BuO, 3141-58-0; NO, 10102-43-9; CH<sub>3</sub>CHO, 75-07-0; (CH<sub>3</sub>)<sub>2</sub>CO, 67-64-1; methoxy radical, 2143-68-2; methyl radical, 2229-07-4.

## Solvent Effects on the Reactivity of Solvated Electrons with Organic Solutes in Methanol/Water and Ethanol/Water Mixed Solvents

Charles C. Lai and Gordon R. Freeman\*

Department of Chemistry, University of Alberta, Edmonton, Canada T6G 2G2 (Received: May 4, 1989; In Final Form: July 10, 1989)

The present work extends the study of solvent effects (*J. Phys. Chem.* **1988**, *92*, 1506 and 5142) to the binary solvents methanol/water and ethanol/water. The composition dependences of energies and entropies of activation for inefficient reactions ( $e_s^- +$  toluene or phenol) are quite different from those for efficient reactions ( $e_s^- +$  nitrobenzene or acetone). In ethanol/water, the inefficient reaction of  $e_s^-$  with toluene makes an interesting change from being mainly entropy driven in pure water solvent ( $\Delta S_2^\ddagger = -51$  J/(mol·K) and  $E_2 = 18$  kJ/mol) to being mainly enthalpy driven in pure ethanol ( $E_2 = 30$  kJ/mol and  $\Delta S_2^\ddagger = -11$  J/(mol·K)). Correlations of  $e_s^-$  reactivity with solvent viscosity and dielectric permittivity are discussed.

### Introduction

The solvent structure of alcohol/water mixtures can manifest itself in a large variety of physical properties,<sup>1-5</sup> including the optical absorption energy of solvated electrons.<sup>6</sup> We have investigated the kinetic behavior of solvated electrons with polar and charged solutes in water mixtures with primary,<sup>7,8</sup> secondary,<sup>9,10</sup> and tertiary alcohols.<sup>11,12</sup> Differences of kinetic behavior within and between different alcohol/water series are due to differences in diffusion rates of the reactants, solvation energies of the electrons, and dielectric properties of the medium. The size and rigidity of the alkyl group on the alcohol molecule seem to have a direct influence on these factors.

The present work extends the study of solvent structure effects on the reactivity of solvated electrons to the water mixtures of the two smallest alcohols, methanol and ethanol. Reaction rate constants of solvated electrons with scavengers of different efficiencies are reported as a function of solvent composition and temperature.

### Experimental Section

**Materials.** Methanol (Aldrich, spectrophotometric grade, Gold Label, 99.9%) was treated for 3 h under argon (Linde, ultrahigh-purity grade, 99.999%) with sodium borohydride (Fisher

TABLE I: Symbols in Figures 1-4, Representing Mole Percent of Water in Methanol or Ethanol

symbol	% H <sub>2</sub> O	symbol	% H <sub>2</sub> O	symbol	% H <sub>2</sub> O
×	0	▼	45	□	95
◇	10	△	60	◇	97
◆	15	▲	70	●	98
▽	20	▣	80	●	99
+	30	■	90	○	100

Scientific, reagent grade; 1 g/L of methanol) at 328 K. It was then fractionally distilled under argon, through a 52 × 2.5 cm column packed with 6-mm glass beads, discarding the first 20% and last 35%. The middle fraction was collected and kept in an argon-pressurized syphon system. The water content determined by Karl-Fisher titration was 0.04 mol %.

Absolute ethanol (reagent grade) was obtained from the U.S. Industrial Chemical Co. Experience had shown this to be the best available,<sup>13</sup> having reported maximum impurity levels of 50 ppm of water, 5 ppm of methanol, and less than 1 ppm of benzene, halogen compounds, or carbonyl compounds. Treatment by the purification method used for methanol resulted in no improvement in purity. The water content measured by Karl-Fisher titration was 0.04 mol %.

The solvated electron half-life after a 100-ns pulse of 1.9-MeV electrons ( $\sim 2 \times 10^{16}$  eV/g) at 298 K was 4 μs for methanol and 6.5 μs for ethanol.

Water was purified in a Barnstead Nanopure II ion-exchange system. The  $e_s^-$  half-life after a 100-ns pulse of radiation was 20 μs.

Toluene (Aldrich, Gold Label) was distilled over sodium under argon. Phenol (Aldrich, 99+%) was sublimed three times under reduced pressure (100 Pa) at 308 K.

Nitrobenzene (Aldrich, 99+%, Gold Label) and acetone (Aldrich 99+%, spectrophotometric grade, Gold Label) were used as received.

**Techniques.** Sample preparation and spectrophotometry for solute concentration measurements are as described in ref 7. Methods of irradiation, dosimetry, and optical measurements were

(1) Symons, M. C. R.; Blandamer, M. J. In *Hydrogen-Bonded Solvent Systems*; Covington, A. K.; Jones, P., Eds.; Taylor and Francis: London, 1968.

(2) Bertolini, D.; Cassettori, M.; Salvetti, G. *J. Chem. Phys.* **1983**, *78*, 365.

(3) Nakanishi, K.; Ikari, K.; Okazaki, S.; Touhara, H. *J. Chem. Phys.* **1984**, *80*, 1656; **1984**, *81*, 4065.

(4) Perl, J. P.; Wasan, D. T.; Windsor, P., IV; Cole, R. H. *J. Mol. Liq.* **1984**, *28*, 103.

(5) Madigosky, W. M.; Warfield, R. W. *J. Chem. Phys.* **1987**, *86*, 1491.

(6) Leu, A. D.; Jha, K. N.; Freeman, G. R. *Can. J. Chem.* **1982**, *60*, 2342.

(7) Mahan, Y.; Freeman, G. R. *J. Phys. Chem.* **1985**, *89*, 4347.

(8) Mahan, Y.; Freeman, G. R. *J. Phys. Chem.* **1987**, *91*, 1561.

(9) Mahan, Y.; Freeman, G. R. *Can. J. Chem.* **1988**, *66*, 1706.

(10) Senanayake, P. C.; Freeman, G. R. *J. Chem. Phys.* **1987**, *87*, 7007.

(11) Senanayake, P. C.; Freeman, G. R. *J. Phys. Chem.* **1987**, *91*, 2123.

On p 2125, the values of  $R_e + R_s$  in zone c should read 1.2 nm for *t*-BuOH/water and 1.0 for 1-PrOH/water. These are larger than the 0.28-nm radius of nitrobenzene, so the reaction occurs at essentially every encounter.

(12) Senanayake, P. C.; Freeman, G. R. *J. Phys. Chem.* **1988**, *92*, 5142.

(13) Akhtar, S. M. S.; Freeman, G. R. *J. Am. Chem. Soc.* **1971**, *75*, 2756.